Journal of Applied Polymer Science

# High-mechanical-strength ferrohydrogels with a magnetically dispersed phase as multifunctional crosslinkers

**Yanzhao Zhu,[1] Zhongkui Wu,[1] Hanmin Lu,[1] Zhi Yue[2]**

[1]School of Materials Science and Engineering, Wuhan University of Technology, Luo Shi Road No. 122, Hong Shan District, Wuhan 430070, China

[2]School of Pharmacy, University of Maryland, 20 Penn Street, Room S612, Baltimore, Maryland 21201

Correspondence to: Z. Wu (E-mail: zkwu@whut.edu.cn)

**ABSTRACT:** In this article, we report a facile strategy for preparing high-mechanical-strength ferrohydrogels containing magnetic nanoparticles homodispersed by a thermodynamically stable Pickering emulsion (PE). After the monomers were mixed with the PE, including methacryloxy propyl trimethoxyl silane emulsified by ferric oxide ($Fe_2O_3$) nanoparticles as the dispersed phase, hydrogels were synthesized by free-radical polymerization. In contrast to conventional hydrogels crosslinked by a molecular crosslinker, in our new approach, the magnetic PE particles served as individual, multifunctional crosslinkers. Characterizations of the swelling behavior, the mechanical properties, and other properties indicated that our ferrohydrogels exhibited outstanding physical performances that were superior to those of traditional hydrogels and magnetic responsiveness. These ferrohydrogels may have applications in soft and controllable actuators. © 2015 Wiley Periodicals, Inc. J. Appl. Polym. Sci. **2015**, *132*, 41950.

**KEYWORDS:** emulsion polymerization; gels; hydrophilic polymers; magnetism and magnetic properties; mechanical properties

Received 17 September 2014; accepted 2 January 2015

**DOI: 10.1002/app.41950**

## INTRODUCTION

The introduction of an inorganic fine grain into the three-dimensional (3D) network of a hydrogel can incorporate additional optical, electric, magnetic, or biological functionalities into these soft and elastic materials with tunable water contents. In particular, the embedding of magnetic nanoparticles (MNPs) into hydrogels can lead to magnetoresponsive hydrogels called *ferrogels*. The tunable deformation and swelling/deswelling of ferrogels in external magnetic fields make biomedical applications that call for noncontact controllable stimulus response possible.[1,2] Therefore, ferrogels may have potential applications in the manufacturing of soft actuators for 3D tissue constructs[3] and the controlled delivery of therapeutics.[4]

Approaches for ferrogel preparation, including blending, *in situ* precipitation, and the grafting-onto method, have been recently discussed.[5] The primary process of blending is to mix dispersed MNPs with a hydrogel precursor solution, and ferronanos would consequently get encapsulated into the hydrogel. This method was, for example, adopted by Liu *et al.*[6] to fabricate poly(*N*-isopropyl acrylamide)/$Fe_2O_3$ magnetic hydrogels. To obtain magnetism, the prepared ferrofluid was mingled with *N*-isopropyl acrylamide solution before suspension polymerization. This is a facile method as the preparation and encapsulation of MNPs are performed separately. However, a uniform distribution of MNPs within hydrogels cannot be guaranteed as the MNPs might diffuse out of the 3D network during swelling. *In situ* precipitation takes the hydrogel network as a chemical reactor, and MNPs are generated by the addition of precipitating agents to the networks containing iron salts.[7,8] Although the dispersion of MNPs from *in situ* precipitation is better than blending, there is little improvement in the reduction of ferronanos diffusion.[5] Consequently, a loss of magnetic particles and the limited mechanical performance therefrom are inevitable. This leads to a rise of the grafting-onto method. As its name suggests, in grafting-onto, magnetic particles are chemically connected to a polymer network. This method, which was used by Fuhrer *et al.*[9] to chemically modify C/Co nanoparticles, has enabled nanomagnets to be crosslinked with the polymer backbone. Nevertheless, the limited strength of hydrogels still holds back their application as actuators. Additionally, the relatively complicated, long process, and high cost of chemical modifications limit its broad applications.

In Messing *et al.*'s[10] study, surface-functionalized magnetic particles with methacrylic groups were used to make multifunctional crosslinkers in the absence of a conventional molecular one [e.g., methylene bisacrylamide (MBA)]. Their ferronanos

Additional Supporting Information may be found in the online version of this article.

were surface-functionalized with a shell containing unsaturated methacrylic groups; this ensured covalent coupling with the hydrogel matrix during the polymerization. However, the uniform distribution of the multifunctional crosslinkers in Messing *et al.*'s[10] work is to be doubted as the homogeneity of their hydrogel network could only be seen on a larger scale (ca. 5$\mu$m) from their transmission electron microscopy characterization; this led to a limited strength. As suggested by Haraguchi and Takehisa[11] a decade ago, a high mechanical strength is accessible with a relatively low crosslinking density and a relatively high intercrosslinking molecular weight (or long intercrosslinking distance). In their study, a nonmagnetic hydrogel was prepared by *in situ* free-radical polymerization with a specific solution in which inorganic clay acted as a polyfunctional crosslinker. Inorganic clay was uniformly dispersed in such a system, and the resulting hydrogel overcame the limitations of conventional chemically crosslinked polymer networks.

Consequently, the strength of the ferrogels were enhanced when the magnetic disperse phase in the emulsion was crosslinkable. Such insights have inspired an in-depth revisit of existing research. The physical incorporation of ferronanos into hydrogels without covalent bonding, as done by Liu *et al.*,[6] could not afford considerable mechanical properties. Although magnetic particles were made crosslinkable by Messing *et al.*,[10] low crosslinking density could not be realized due to nonuniform distribution of magnetic particles. As a result, the higher mechanical strength of ferrogels is accessible with increased homogeneity in the distribution of magnetic particles.

In this respect, Sacanna *et al.*'s[12,13] work would support improvement. They successfully made several thermodynamically stable oil-in-water Pickering emulsions (PEs) with decent monodisperse nanodroplets. Such emulsions circumvent inhomogeneous distribution. Notably, such spontaneously emulsifiable PEs are completely different from Liu *et al.*'s.[6] In another study, Sacanna and Philipse[14] group adopted this emulsion to manufacture core–shell colloids by a one-pot way as the oil phase may provide many double bonds, which may link with many long polymer chains. So, it is promising to introduce this system to hydrogel preparation, as long as a hydrophilic monomer is used.

In this article, we report a novel and simple approach for fabricating ferrogels with a high mechanical performance by the gelatinization of a PE containing acrylamide (AAm). Inspired by Sacanna's work, we initiated the polymerization of AAm and modified 3-methacryloxypropyl trimethoxysilane (TPM) in a special emulsion system consisting of TPM as the oil phase, AAm aqueous solution as the aqueous phase, and magnetite nanoparticles as the disperser to prepare ferrohydrogels. The swelling behavior, mechanical performance, and other characterizations were examined to determine the structure of the hydrogel.

## EXPERIMENTAL

### Chemicals

$FeCl_2{\cdot}4H_2O$, $FeCl_3{\cdot}6H_2O$, $NH_4OH$ (25%), $HNO_3$ (63%), $Fe(NO_3)_3{\cdot}9H_2O$, tetramethyl ammonium hydroxide (25%, aqueous), potassium persulfate (KPS; 99%), HF (aqueous, 48%), HCl (aqueous, 37%), AAm, and sodium dodecyl sulfate (SDS) were purchased from Sinopharm Chemical Reagent Co., Ltd. *N,N,N′,N′*-Tetramethylethylenediamine (TEMED) and MBA were purchased from Aladdin Reagent Co., Ltd. TPM were obtained from Wuhan Hualun Chemical Factory. Deionized water was used for all of the experiments in this study.

### Synthesis of the $\gamma$-$Fe_2O_3$ Nanoparticles

The preparation of maghemite ($\gamma$-$Fe_2O_3$) was conducted by a two-step method based on the method of Massart.[15] First, magnetite ($Fe_3O_4$) nanoparticles were prepared under a nitrogen atmosphere by the alkaline precipitation of ferrous chloride and ferric chloride (molar ratio = 1:2). The precipitates were decanted three times and redispersed in deionized water. Then, the dispersion was acidified by $HNO_3$ (200 mL, 2*M*) under stirring for 0.5 h. The acidified precipitates were collected by decantation and boiled with $Fe(NO_3)_3$ (200 mL, 2*M*) for 2 h. After decantation, the collected maghemite precipitates were redispersed by the addition of tetramethyl ammonium hydroxide (aqueous, 25%); this led to a stable ferrofluid of maghemite nanoparticles (Figure S2, Supporting Information).

### Fabrication of the $Fe_2O_3$ Nanoparticle-Stabilized Pickering Emulsion

The stabilized maghemite nanoparticles dispersion (dispersants and water phase of the PE) was added to deionized water to a concentration of 5 mg/mL; this was followed by the addition of a given volume (150–400 $\mu$L) of TPM (oil phase). The oil–water mixture was spontaneously emulsified at about 4°C for about 24 h (Figure S1, Supporting Information). The composition of the PEs is listed in Table S1 in the Supporting Information.

### Preparation of the TPM-Linked PAAm and MBA-Linked Hydrogels

The PE ferrohydrogels were synthesized from 10 mL of aqueous particle dispersion with 25% (m/m) AAm. We initiated the polymerization by an initiator (KPS, 5 mg) and an accelerator (TEMED, 25$\mu$L) by warming up the sample to room temperature. The reaction was completed within 5 h. This fabrication strategy is illustrated in Figure 1. For comparison, a classic MBA-linked PAAM hydrogel (CL gel) and traditional-emulsion PAAM hydrogel (TE gel) were also prepared under similar conditions of gel made from PE gel (i.e., 0.15 g of MBA replaced 300 $\mu$L of TPM in the CL gel, and SDS dispersion replaced the $Fe_2O_3$ dispersion in the TE gel, see Table S1, Supporting Information). The traditional emulsion of the TE gel was emulsified by traditional dispersants (SDS = 0.015 mol/L).

### Characterization

Transmission electron microscopy images of the maghemite nanoparticles and the PE were taken with a JEM-2100F STEM/EDS instrument. The samples were prepared by drop-casting on a carbon grid. X-ray diffraction was performed on an X'Pert PRO diffractometer equipped with monochromatic Cu K$\alpha$ radiation with a wavelength of 1.5406 Å. Scanning electron microscopy (SEM) images of the PE ferrohydrogel was taken by S-4800. After lyophilization, the hydrogels were sputter-coated with gold. Particle size analysis of the PE was performed with a ZEN1600 from Malvern Instruments, Ltd. The PE was diluted by a factor of four.

The tensile mechanical properties of the hydrogels with different compositions were measured by a WDW-05 electronic universal

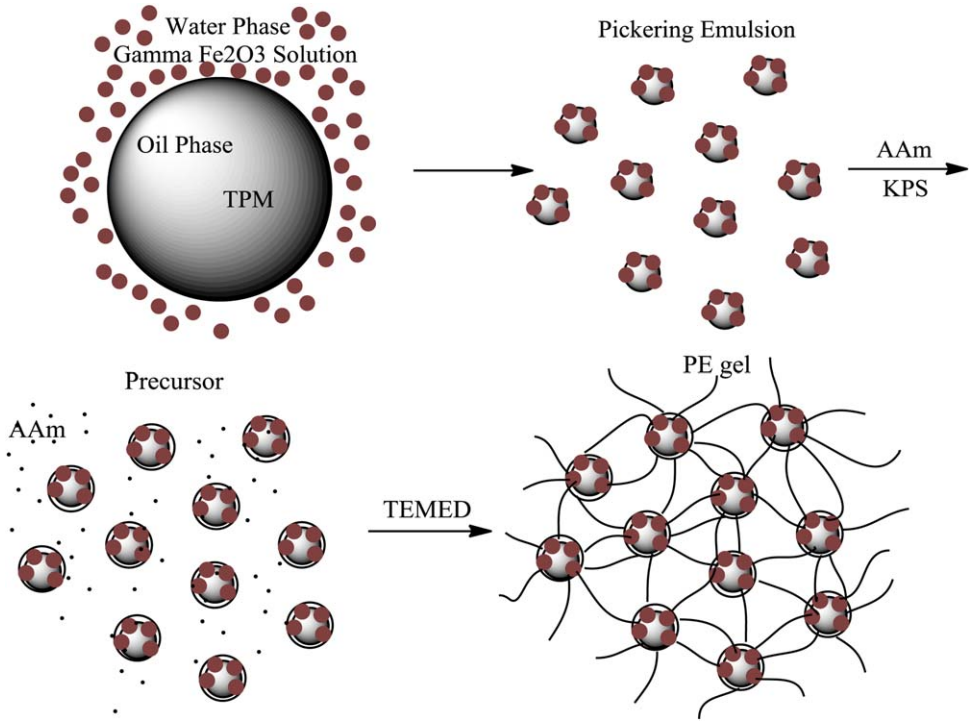


**Figure 1.** Preparation of the emulsion-linked hydrogel. [Color figure can be viewed in the online issue, which is available at wileyonlinelibrary.com.]

material testing instrument. Samples that were 10 mm long and 4.5 mm wide were characterized at 25°C at a crosshead speed of 100 mm/min. The compression mechanical properties were mainly determined with an M-30 electronic universal material testing instrument. The compression test of the MBA-linked hydrogel was conducted with a WDW-05 electronic universal material testing equipment because of its broader measuring range. Samples that were 20 mm long and 15 mm wide samples were characterized under 25°C and a crosshead speed of 5 mm/min. Each type of hydrogel was tested at least three times, and the results were averaged.

Swelling was performed by the immersion of dried hydrogels into a large excess of deionized water (pH 7) at 25°C. The samples were weighed at a fixed interval of time. The swelling ratio ($W$) was calculated by the following equation:

$$W = \frac{(W_s - W_d)}{W_d} \quad (1)$$

where $W_s$ and $W_d$ are the weights of the wet hydrogel at a given time during the swelling and of the dry hydrogel, respectively.

## RESULTS AND DISCUSSION

### Preparation

The TPM-linked hydrogels were prepared by the following steps. As the methacrylate oil phase and charged colloids could self-assemble into thermodynamically stable, opaque emulsions of monodisperse droplets in aqueous solution.[12,13] TPM and a maghemite particle dispersion were mixed under appropriate conditions to form PEs with magnetic disperse phases. AAm and the initiator (KPS) were consecutively dissolved in the emulsion to form a precursor. The accelerator (TEMED) was then added to initiate the radical polymerization in the presence of nitrogen. The magnetic disperse phase (stabilized TPM droplets), acting as multifunctional crosslinkers, could crosslink with AAm to form a uniform network structure. The whole procedure is schematically represented in Figure 1.

### DTS Characterization

Figure 2(a) shows the disperse-phase size distribution of the PE (PE2). The *Z*-average size of the TPM disperse phase was only 107 nm with a low PDI of 0.114; this indicated monodispersion (Figure S3, Supporting Information). After the addition of a modest amount of AAm (2.5 mol/L) and the initiator KPS (0.004 mol/L) into the emulsion, the distribution profiles of the suspension rightshifted a bit [Figure 2(b,c)]. However, the *Z*-average sizes and poly-dispersity index (PDI)s were still less than 200 nm and 0.3, respectively. So, AAm and KPS had relatively little impact on the emulsion stability, and TPM was still monodispersed and uniformly distributed. This was expected because of the following reasons. First, the TPM disperse phase could absorb some AAm as AAm had an oleophilic double bond. Second, the initiator (KPS) reduced the exclusive forces among the TPM disperse phase, so the TPM disperse phase could reaggregate. As such, a suspension structure was maintained in the polymerization, and the final product was a gel rather than a viscous fluid; this indicated that both the AAm and TPM disperse phase were involved in the reaction. As both AAm and TPM were bifunctional, the 3D structure could not be attained if TPM was not integrated into the disperse phase to afford more functionality. Additionally, as the oil-phase TPM could partially hydrolyze into larger multifunctional molecules, the attained crosslinked material was not easy to break under stress. It is noteworthy that excessive initiator could destroy the

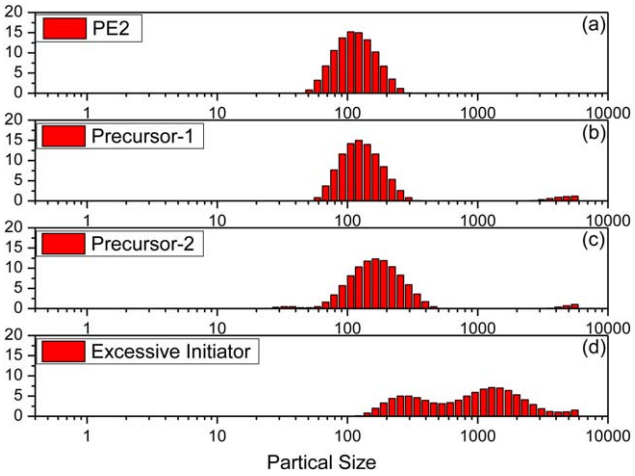


**Figure 2.** Size distribution of the mixture from different phases of the preparation: (a) size distribution of the PE (PE2), (b) size distribution of the precursor after the addition of AAm, (c) size distribution of the precursor after the addition of KPS, and (d) PE with excessive initiator. [Color figure can be viewed in the online issue, which is available at wileyonlinelibrary.com.]

stable emulsion [Figure 2(d)], as a large amount of electrolytes could impair double-electrode layers to remove exclusive forces among the TPM disperse phase.

### SEM Characterization

Figure 3(a1) shows an SEM sectional view of the PE gel, from which many polygons could be observed. These polygons with holes were generated because of a loss of water. These dimple-like holes were capable of scattering stress. There existed a large space between the polymer chains to accommodate a large amount of water. So, the PE gel was stress resistant. The existence of some filaments generated during truncation indicated good ductility. The 3D structure was still preserved, even when the gel was partially destroyed, so the gel could withstand large tensile stresses.

Figure 3(a2) shows a close-up view of the region circled by the red curve in Figure 3(a1). There were lots of small off-white dots uniformly distributed on the cross section. Most of these dots had a diameter between 100 and 200 nm; this was in line with the previous DTS results. We, therefore, considered these homodispersed dots as the TPM disperse phase in the PE gel. To further confirm our hypothesis, we tested a control system. Nanoferros in the PE2 gel were replaced with SDS in the TE gel, and the other conditions were kept untouched. The SEM graph showed that TPM aggregates were polydispersed and irregularly distributed in the gel [Figure 3(b)]. Flaws were created during lyophilization; this indicated poor mechanical properties.

### Dissolution Analysis

On the basis of Messing *et al.*'s[10] method, a brown, water-swollen hydrogel was immersed in concentrated hydrochloric acid (37 wt %) at room temperature. The hydrogel was bleached within 10 min, but it was not dissolved. Some off-white dots were still observable in SEM [Figure 4(a)]. As these small dots acted as crosslinking points, the gel still maintained its 3D structure. After the acid was washed out by deionized water, the hydrogel was immersed in hydrofluoric acid (40 wt %), and the network structure was quickly destroyed. This was expected because hydrofluoric acid could break Si—O bonds functioning as crosslink points. Compared with Messing's product, our hydrogel lost its nanoferros in hydrochloric acid with a higher concentration and broke in hydrofluoric acid with a higher concentration; this indicated that it had a higher structural stability.

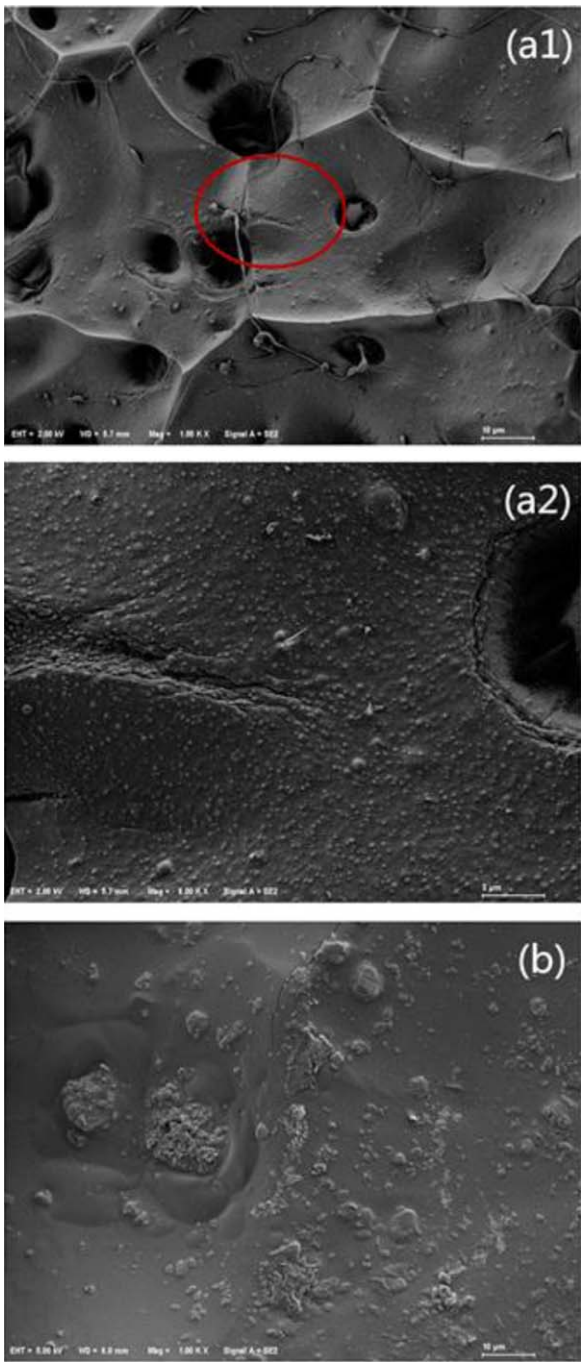


**Figure 3.** SEM graph of the PE and TE gels: (a1) SEM of the PE gel at 10 $\mu$m, (a2) close-up view of the red curve circled region in a1 at 2 $\mu$m, and (b) SEM of the TE gel at 10 $\mu$m. [Color figure can be viewed in the online issue, which is available at wileyonlinelibrary.com.]

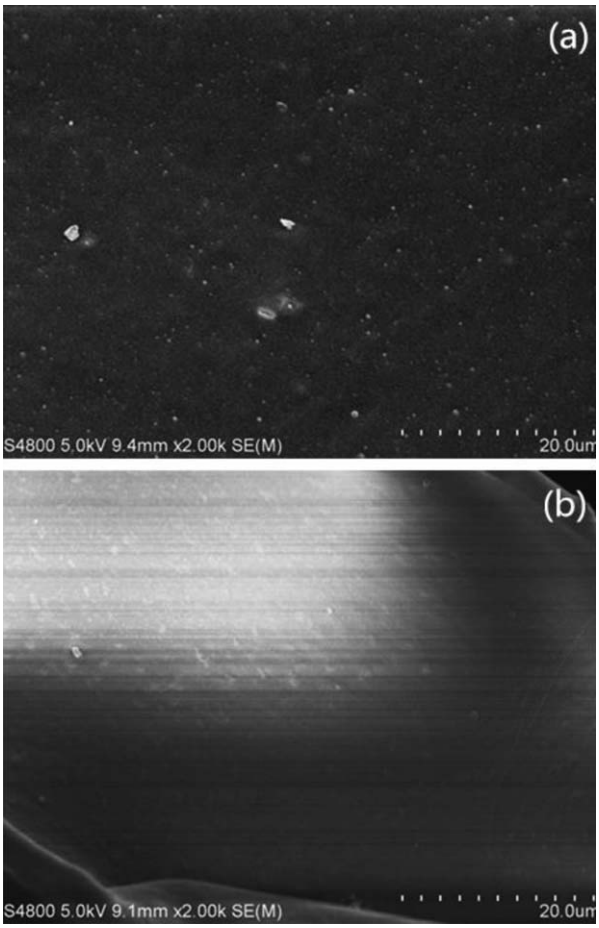


**Figure 4.** Dissolution analysis of the PE gel: (a) treated by concentrated hydrochloric acid (37 wt %) and (b) treated with an aqueous solution with several drops of hydrofluoric acid.

The hydrogel did not completely dissolve in a dilute hydrofluoric acid aqueous solution over several hours. However, those off-white dots that were observed previously were no longer detectable in SEM [Figure 4(b)]. This was attributed to the formation of a special structure. In PE gels, the TPM disperse phase was embedded into PAAm to form a core–shell structure, and this slowed down acid penetration. Additionally, as ferrona-nos had a higher affinity with TPM (with a smaller contact angle between the ferronanos and water than that between the ferronanos and TPM), TPM encapsulated ferronanos to attenuate the erosion of hydrochloric acid. We have demonstrated that our hydrogel could resist a relatively harsh environment (room temperature, pH 2–10) without a loss of magnetic particles for a long time (PAAm dissolved above pH 10).

### Swelling Test

Figure 5 illustrates the swelling ratios of the CL, TE, and PE hydrogels with different TPM contents. These hydrogels did not dissolve in water but swelled to equilibrium (see plateaus in Figure 5). Compared to the other two, the PE hydrogels displayed a prominent swelling capacity. In particular, the equilibrium swelling ratio of the PE1 hydrogel reached 131, the value of which was more than seven times those of the CL and TE hydrogels.

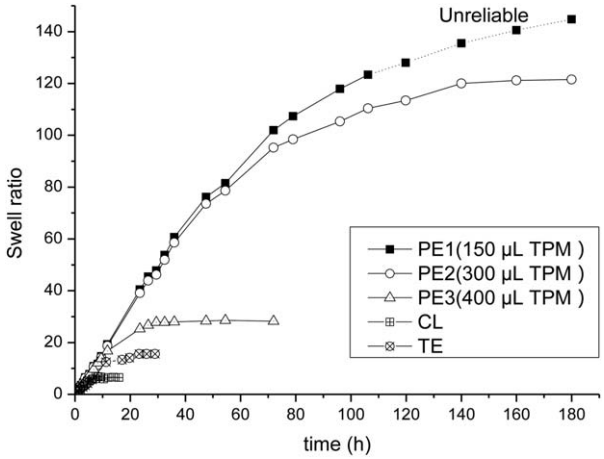


**Figure 5.** Swelling ratios of the CL, TE, and PE hydrogels with different TPM contents as a function of time. The final segment of the PE1 curve in the dotted line is unreliable because of its low strength.

Microscopically, the swelling of a nonelectrolyte hydrogel is produced by the direct diffusion of small molecules in solvent into a hydrogel network and/or the movement of polymer chains in a solvent. If only the former participates, the swelling should obey Fickian diffusion as described by eq. (2):

$$\frac{M_{ta}}{M_{\infty}} = kt^{n} \tag{2}$$

where $M_{ta}$ is the weight of water absorbed at time $t$, $M_{\infty}$ is the weight of water absorbed at equilibrium, $n$ is the characteristics exponent of swelling, and $k$ is a constant.[16]

We used this equation to analyze the swelling behavior of our hydrogels. The equation held at a swelling ratio below 60% ($M_{ta}/M_{\infty} \leq 0.6$). The value of $n = 0.5$ is a characteristic for Fickian diffusion, whereas $0.50 \leq n \leq 1$ indicates anomalous (or non-Fickian) diffusion. Figure 6 plots $\ln(M_{ta}/M_{\infty})$ versus $\ln t$ for all of hydrogels, as shown in Figure 5. The slopes of these lines give $n$ of 0.55 for the CL gel and 0.84–0.91 for PE1, PE2, PE3, and TE gels; this indicated non-Fickian swelling of the PE and TE hydrogels.

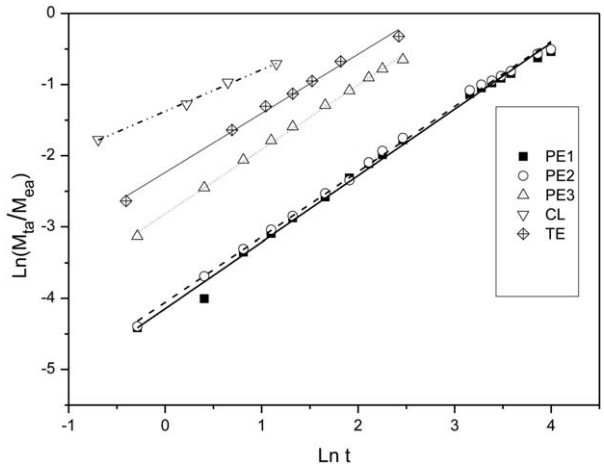


**Figure 6.** $\mathrm{Ln}(M_{ta}/M_{\infty})$ versus $\ln t$ for the CL, TE, and PE hydrogels with different TPM contents.

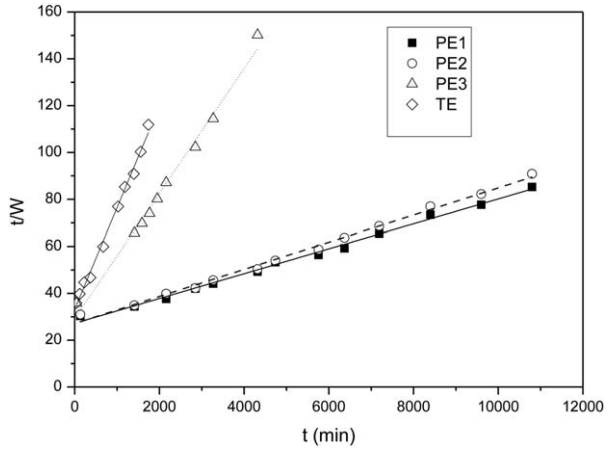


**Figure 7.** $t/W$ as a function of $t$ for the TE and PE hydrogels with different TPM contents.

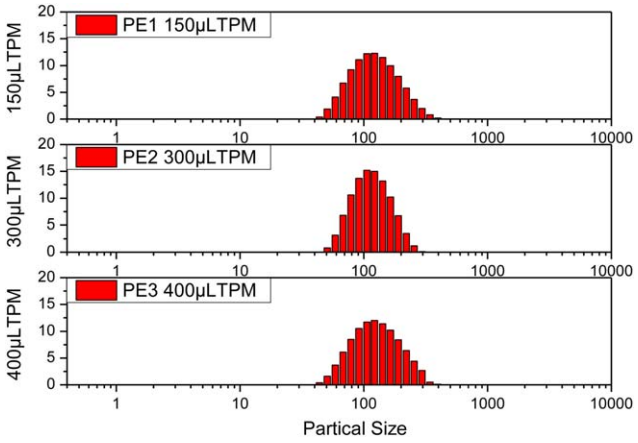


**Figure 8.** Influence of TPM on the PE micelle diameter: (a) PE1 (150 $\mu$L of TPM), (b) PE2 (300 $\mu$L of TPM), and (c) PE3 (400 $\mu$L of TPM). [Color figure can be viewed in the online issue, which is available at wileyonlinelibrary.com.]

Non-Fickian swelling obeys Schott's second-order swelling kinetics, which is described by eq. (3):

$$\frac{dW}{dt} = k_s(W_\infty - W)^2 \tag{3}$$

where $W$ is the swelling ratio at time $t$, $W_\infty$ is the swelling ratio at equilibrium, and $k_s$ is the swelling rate constant. Through the application of initial conditions ($t = 0$, $W = 0$), eq. (4) could be rewritten as follows:

$$\frac{t}{W} = A + Bt \tag{4}$$

where $A = 1/k_s W_I^2$ and $B = 1/W_\infty$.[17]

Figure 7 shows a good linear relation between $t/W$ and $t$ for the PE1, PE2, PE3, and TE gels; this indicates that the swelling process of the PE and TE hydrogel followed the Schott's model. As the Schott's model held when both the diffusion of water and the relaxation of macromolecular chains dominated swelling; the movement of polymer chains in the solvent gave access to the slack and expansion of the PE hydrogels.

The distance between two crosslinking points was about 500 nm in the PE gel [Figure 2(a2)]. Although in the CL gel, such a distance was less than 50 nm (one MBA molecule was surrounded by 400 AAm molecules, and an AAm molecule was smaller than 0.1 nm) provided that MBA was evenly distributed in the gel; this indicated different swelling mechanisms for the CL and PE gels. A hydrogel with a smaller molecular weight among crosslinking points chains was hard to expand to harbor more water (like CL gel) and vice versa (like PE gel).

Figure 5 indicates that the swelling ratio of the PE gel decreased with increasing TPM content. Two attributes accounted for this behavior. First, as shown in Figure 8, the growth of the

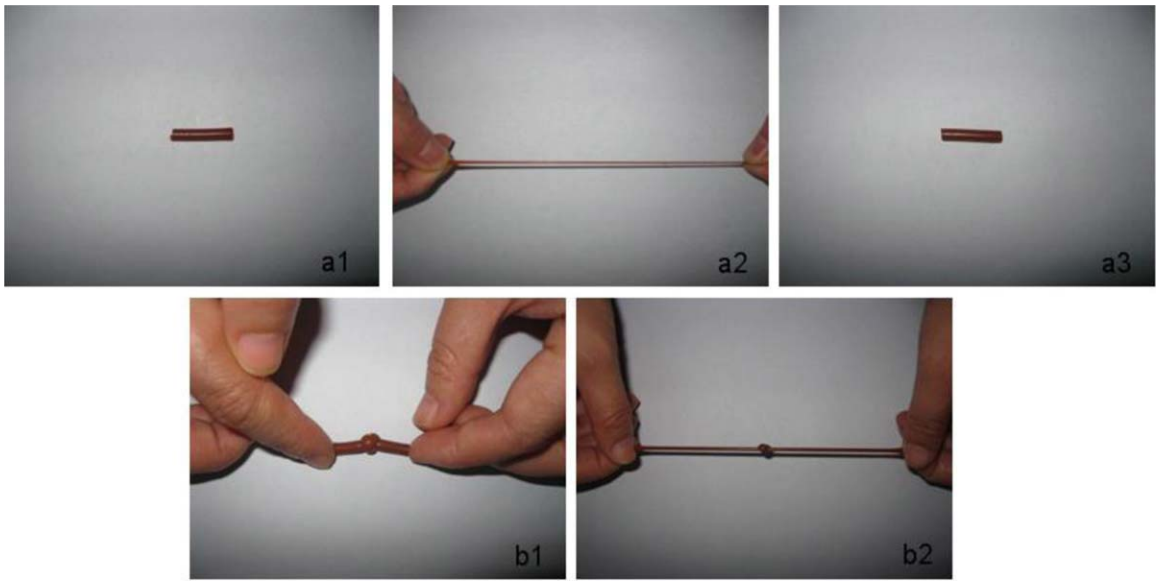


**Figure 9.** Mechanical properties of a PE hydrogel (PE3): (a1–a3) before, in, and after elongation and (b1, b2) knotting and after-knotting stretching. [Color figure can be viewed in the online issue, which is available at wileyonlinelibrary.com.]

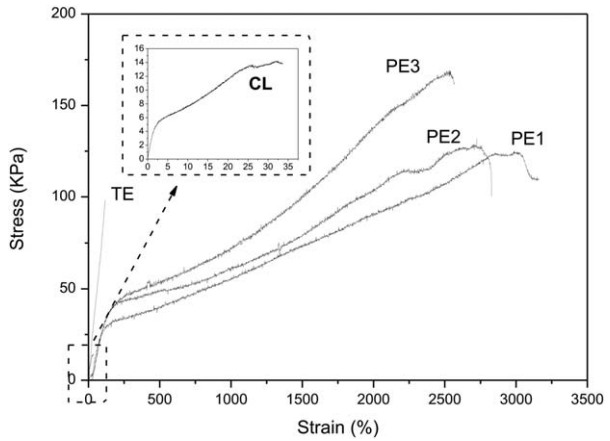


**Figure 10.** Tensile stress–stain curves of the CL, TE, and PE hydrogels with different TPM contents. The CL hydrogel showed a rather low tensile strength of 14.2 kPa and an elongation at break of 34%. The TE hydrogel showed a low elongation at break of 178%. The PE hydrogels exhibited relatively high tensile strength (>150kPa) and an excellent elongation at break (>2000%). PE1 even reached an elongation at break of 3697%, which was more than 108 times higher than that of the MBA-linked hydrogel. The TPM-linked hydrogels had much higher tensile properties than the TE hydrogel.

disperse-phase diameters was not proportional to the growth of the TPM content; this suggested that the number of crosslinking points increased with increasing TPM. Second, as mentioned before, when the surfaces of the TPM disperse phase were covered with a layer of PAAm, the higher TPM content increased the AAm content in the shells and suppressed its chance of bridging crosslinking points. This result clarified that the chains between the effective crosslinking units (TPM disperse phase) played a key role in the swelling of the nonelectrolyte hydrogel.

### Mechanical Properties

PE gels were tested to withstand various stresses, such as stretching, knotting, and stretching after knotting by large deformation (Figure 9).

The tensile stress–stain curves (Figure 10) of the PE hydrogels revealed good tensile strength (>150kPa) and excellent elongation at break (>2000%). These fabulous properties may have originated from their unique structure. To better understand this, we performed two control experiments. First, we replaced the nanoferros in the PE gel by SDS (the other conditions remained untouched) to prepare the TE gel. SDS could partially disperse TPM to a certain extent (100 nm–1 $\mu$m) under mechanical stirring [Figure 3(b)]. Such a system also has multifunctional crosslinkers from the partial hydrolysis of TPM. However, the elongation at break of this TE gel was much lower than that of the PE gel (Figure 10). The asymmetric TPM in suspension led to the nonuniformity of crosslinking points after polymerization. After tensile stress was exerted, the region in the TE gel containing fewer crosslinking points fractured first. Second, TPM in the PE2 gel was replaced by MBA and the other conditions remained unchanged. However, neither the elongation at break nor the tensile strength was good (Figure 10). As MBA was a small molecule with two double bonds, the resulting MBA-linked hydrogel had a less ordered network structure and a relatively higher crosslinking point density; this, in turn, resulted in an uneven distribution of stress.[11] Moreover, the ferronanos were not combined with crosslinkers or monomers, so swelling could easily destroy its structure. Nevertheless, in the TPM-linked hydrogel the maghemite-stabilizing TPM disperse phase still functioned as a multifunctional crosslinker. These disperse phases could be distributed evenly in the reactants and brought about the well-distributed effective crosslinking points. The DTS characterization manifested that the diameters of the dispersed phase ranged from 100 to 200 nm, and the addition of monomers and initiator to the PE only induced a slight increment (30–40 nm, Figure 2). Meanwhile, as TPM had a double bond, hundreds of TPM molecules provided hundreds of double bonds to crosslink with other disperse phases by a large amount of monomers. So a relatively low crosslinking density and a relatively high intercrosslinking molecular weight in the network could be guaranteed.

Figure 10 also shows that the tensile strength and elongation at break of the PE hydrogel differed slightly at different contents of TPM. As less TPM led to fewer crosslinking points and larger distances between adjacent maghemite-stabilizing TPM droplets, PE1 was more flexible than PE2 and PE3 as it had a higher elongation at break. However, longer and more flexible free chains between these droplets led to relatively low friction between the polymer chains. Hence, the tensile strength of the TPM-linked gels decreased with reduced TPM content.

The PE hydrogels also exhibited excellent compressive properties (Table I) as all of the PE hydrogels could resist a compressive stress of about 17 MPa without fracturing; this stress was more than 90 times higher than that of CL gel (0.18 MPa). As the molecular weight between crosslinking points was inversely proportional to the density of the crosslinking points, a lower crosslinking density gave more flexible chains to scatter stress

**Table I.** Mechanical Properties of the Hydrogels

| Sample | Fracture tensile stress (KPa) | Elongation (%) | Compressive stress (MPa) | Strain (%) | Appearance after testing |
|---|---|---|---|---|---|
| PE1 | 125 | 3120 | 17.1 | 90 | Recovered |
| PE2 | 127 | 2710 | 17.9 | 90 | Recovered |
| PE3 | 168 | 2534 | 18.5 | 90 | Recovered |
| CL | 14 | 33 | 0.18 | 53 | Fractured |
| TE | 98.3 | 115.2 | 4.78 | 75 | Fractured |

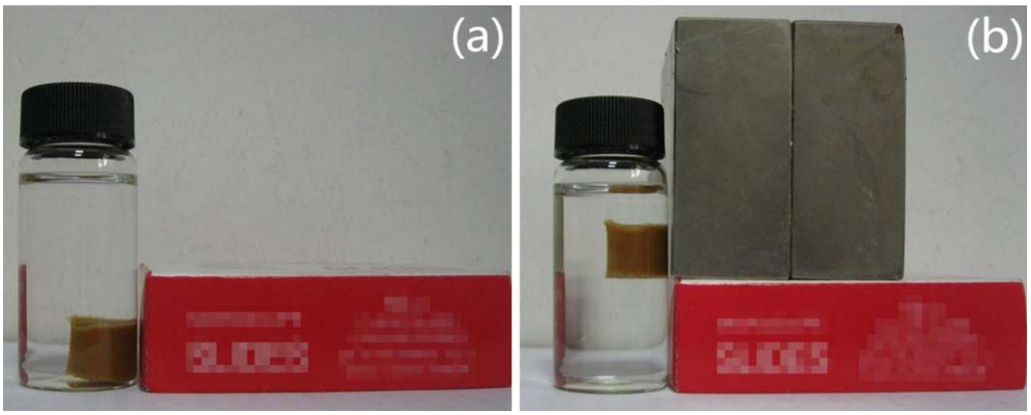


**Figure 11.** Photographs of the composite hydrogel in water (a) without and (b) under an external magnetic field. [Color figure can be viewed in the online issue, which is available at wileyonlinelibrary.com.]

and resist failure. Moreover, the PE gels gave better strength compared to the TE hydrogel. The uniformly distributed TPM in the PE gel was responsible for this, although in the TE gel, an unstable emulsion, including a collective disperse phase of inhomogeneous diameters, was used.

### Magnetic Response Test

The magnetic response test (Figure 11) manifested that the hydrogel, for example, PE2, responded to the external magnetic field. The magnetic microcapsules readily moved up and down with the help of an external magnetic field. We also found that the MNPs retained their properties in the PE hydrogel, as the curve had nearly the same shape as the hysteresis loop (Figure S4, Supporting Information).

## CONCLUSIONS

We prepared a novel magnetic hydrogel (ferrohydrogel) based on a thermodynamically stable PE droplets containing $Fe_2O_3$ nanoparticles. The uniform distribution of crosslinking points in the ferrohydrogel network was confirmed by SEM and DTS characterization. Dissolution experiments showed that the crosslinking in the ferrohydrogels originated from the siloxane-based shell hydrolyzed from TPM. Ferronano-modified TPM droplets acted as individual, multifunctional crosslinkers in the hydrogel and, therefore, conferred the hydrogel high resistance to relatively harsh environments without a loss of ferronanos and fracturing of the 3D network structure. The microscopic characterization of the gel structure suggested a well-defined network structure, which resulted in its fabulous mechanical properties. Control experiments showed that it was nanoferros rather than emulsifiers that changed TPM into crosslinkers and that the structure of our hydrogel was totally different from that of traditional MBA gels. The analysis of the dependence of the swelling degree of the two series of ferrohydrogels on the TPM content indicated the influence of TPM on the network formation and architecture. Overall, our effort to make magnetic hydrogels sheds light on the embedding of MNPs into hydrogels.

## ACKNOWLEDGMENTS

The authors thank Lijun Chen for ZEN1600 from Malvern Instruments, Ltd., and the Wuhan University of Technology material testing center for providing SEM. This work was financially supported by the National Natural Science Foundation of China (contract grant number 50973087/E0310).

## REFERENCES

1. Griffith, L. G.; Swartz, M. A. *Nat. Rev. Mol. Cell Biol.* **2006**, *7*, 211.
2. Meenach, S. A.; Hilt, J. Z.; Anderson, K. W. *Acta Biomater.* **2010**, *6*, 1039.
3. Geckil, H.; Xu, F.; Zhang, X. H.; Moon, S.; Demirci, U. *Nanomed. UK* **2010**, *5*, 469.
4. Liu, T. Y.; Hu, S. H.; Liu, T. Y.; Liu, D. M.; Chen, S. Y. *Langmuir* **2006**, *22*, 5974.
5. Li, Y. H.; Huang, G. Y.; Zhang, X. H.; Li, B. Q.; Chen, Y. M.; Lu, T. L.; Lu, T. J.; Xu, F. *Adv. Funct. Mater.* **2013**, *23*, 660.
6. Liu, H. X.; Wang, C. Y.; Gao, Q. X.; Liu, X. X.; Tong, Z. *Acta Biomater.* **2010**, *6*, 275.
7. Nagireddy, N. R.; Yallapu, M. M.; Kokkarachedu, V.; Sakey, R.; Kanikireddy, V.; Alias, J. P.; Konduru, M. R. *J. Polym. Res.* **2011**, *18*, 2285.
8. Beaune, G.; Menager, C. *J. Colloid Interface Sci.* **2010**, *343*, 396.
9. Fuhrer, R.; Athanassiou, E. K.; Luechinger, N. A.; Stark, W. *J. Small* **2009**, *5*, 383.
10. Messing, R.; Frickel, N.; Belkoura, L.; Strey, R.; Rahn, H.; Odenbach, S.; Schmidt, A. M. *Macromolecules* **2011**, *44*, 2990.
11. Haraguchi, K.; Takehisa, T. *Adv. Mater.* **2002**, *14*, 1120.
12. Sacanna, S.; Kegel, W. K.; Philipse, A. P. *Phys. Rev. Lett.* **2007**, 98.
13. Sacanna, S.; Kegel, W. K.; Philipse, A. P. *Langmuir* **2007**, *23*, 10486.
14. Sacanna, S.; Philipse, A. P. *Adv. Mater.* **2007**, *19*, 3824.
15. Massart, R. *IEEE Trans. Magn.* **1981**, *17*, 1247.
16. Ritger, P. L.; Peppas, N. A. *J. Controlled Release* **1987**, *5*, 23.
17. Schott, H. J. *Macromol. Sci.* **1992**, *31*, 1.